Numerical Simulations of Compressible Two-Component Flows with General Equation of State

Shaban Jolgam [1*] , Ahmed Ballil [2] , Andrzej Nowakowski [3] , Abdulmaged Shati[1]

[1] Mechanical Engineering Department, Faculty of Engineering, University of Zawia, Zawia, Libya

[2] Mechanical Engineering Department, Faculty of Engineering, University of Benghazi, Benghazi, Libya,

[3] Department of Mechanical Engineering, University of Sheffield, Sheffield, UK

*Corresponding author email: shaban.jolgam@zu.edu.ly

ABSTRACT

Numerical simulations of compressible two-component flows with a general equation of state (EOS), written in the form of the Mie-Grüneisen EOS, have been conducted using the diffuse interface method on a structured mesh. The unsteady and inviscid one-dimensional six-equation model of Kapila is employed to describe compressible two-component flows. The model is hyperbolic and non-conservative. The solution of the hyperbolic equations, including the non-conservative equation for the volume fraction evolution, is obtained using an extended Harten-Lax-Leer (HLL) approximate Riemann solver. A general formulation for various EOSs is proposed to enable simulations of a wide range of applications. In which the two constituents are either governed by the same EOS or different types of EOS. In this model, both fluids have the same velocity, but each fluid has its own pressure. Therefore, the pressure relaxation process is performed instantaneously to drive both constituents' pressures towards equilibrium. Several computational test problems were conducted in one and two dimensions to show the ability of the numerical method to simulate such problems. The computed results are presented without introducing spurious pressure oscillations in the method.

Keywords: Compressible multiphase flow, equation of state, shock wave, Godunov's method, approximate Riemann solver.

المحاكاة العددية للتدفقات المضغوطة المكونة من عنصرين مع المعادلة العامة للحالة

شعبان جلغام¹، أحمد بالليل²، أندرو نوفاكفسكي³، عبدالمجيد شتي¹

¹ قسم الهندسة الميكانيكية، كلية الهندسة، جامعة الزاوية، الزاوية ليبيا

² قسم الهندسة الميكانيكية، كلية الهندسة، جامعة بنغازي، بنغازي ليبيا

³ قسم الهندسة الميكانيكية، كلية الهندسة، جامعة شفيلد، شفيلد بريطانيا

ملخـــــص البحـــــث

تم إجراء عمليات محاكاة عددية للتدفقات القابلة للضغط المكونة من عنصرين مع معادلة عامة للحالة (EOS)، مكتوبة في شكل معادلة مي-قرنسين للحالة، باستخدام طريقة الواجهة المنتشرة على شبكة منظمة. تم استخدام نموذج المعادلات

السداسية غير المستقر وغير الواضح لكابيلا لوصف التدفقات القابلة للضغط المكونة من عنصرين. النموذج مبالغ فيه

وغير محافظ. تم الحصول على حل المعادلات الزائدية بما في ذلك المعادلة غير المحافظة لتطور جزء الحجم باستخدام

حل ريمان التقريبي الموسع هارتن–لاكس–لير (**HLL**). تم اقتراح صياغة عامة لمعادلات الحالة المختلفة لتمكن من

إجراء محاكاة مجموعة واسعة من التطبيقات. حيث يتم التحكم في المكونين بنفس معادلة الحالة أو أنواع مختلفة من

معادلات الحالة. تم اشتقاق سرعة الصوت لكل من معادلة الحالة لفان درفال ولكوكران–تشان ولجونس–ولكنس–لي

ولموجات الصدمة. في هذا النموذج، كلا المائعين لهما نفس السرعة ولكن لكل منهما ضغطه الخاص. لذلك، يتم تنفيذ

عملية تخفيف الضغط بشكل فوري لدفع ضغط كلا المكونين نحو الاتزان. تم إجراء العديد من الاختبارات الحسابية في

البعد الواحد والبعدين لبيان قدرة الطريقة العددية على محاكاة مثل هذه المسائل بمعادلات حالة مختلفة بنفس البرنامج،

دون الحاجة إلى تعديله. تم عرض النتائج المحسوبة دون وجود تذبذبات الضغط الزائفة في الطريقة.

الكلمات الدالة: الجريان المضغوط متعدد الأطوار ، معادلة الحالة، موجة الصدمة، طريقة غودونوف، حل ريمان التقريبي.

1. Introduction

Many processes and systems involve multi-component flows. For example, gas mixing for combustion, shock bubble interaction, water under pressure used to cool the nuclear reactor core, coolant spray in cooling towers, and cavitation, which may take place on pump impellers, turbine blades, or marine propellers. Although compressible multi-component flows have been widely investigated, the numerical technique enabling the capture of interfaces using a general equation of state (EOS) remains a challenging problem. The ability of a numerical method to deal with various EOS enables the study of a wide range of applications.

To track or capture the interfaces separating multi-component flows, two main approaches have been developed. They are the Sharp Interface Methods (SIM) and the Diffuse Interface Methods (DIM). In the SIM approach, the interfaces are considered a sharp (non-smeared) discontinuity in the physical or thermodynamic properties of the fluids in contact. In the DIM approach, the interfaces are considered a diffused zone over a narrow band. To deal with multi-component flows using the SIM approach, various methods have been used with different types of EOSs. For example, in [1], the front tracking method was implemented to simulate detonation problems with complex EOS governing real gases. In [2], the level set method was used to simulate a broad set of test problems where the fluids are governed by the stiffened EOS, and in [3], the interface solver based on the coupled level set and volume-of-fluid method was used for simulating an underwater explosion where water is governed by Tait's EOS.

On the other hand, the simplicity of the DIM to deal with coalesce or breakup among different phases or fluids has led many researchers to consider this approach. In a recent study [4], the phase-field model and corresponding numerical method were developed to simulate a compressible multiphase flow. Some studies refer to this method as DIM. In early developments, to simulate material interfaces in compressible multi-fluids, various models have been used, for example, the mass fraction model, and the Gamma model. However, they suffered from unphysical oscillations in mass fraction and pressure at material interfaces. In [5], the mass fraction model was used in which a numerical flux modification was introduced. It guarantees the positivity of the mass fraction but produces pressure oscillations. In [6], the Gamma model based on a non-conservative scheme was used to avoid pressure oscillations, which guarantees mass fraction positivity but cannot handle strong shock waves. Karni improved her method to capture strong shock waves [7]. The method was established using a level set technique to trace the interface location; the pressure at the interface is calculated using the primitive variable formulation of the Euler equations. However, their major drawbacks are due to conservation errors, which produce inaccurate internal energy and temperature at the interface. Moreover, they are not easy to be applied with various equations of state. In [8], a quasi-conservative method based on the mass fraction model was used to prevent spurious oscillations in pressure. Based on the basic idea of Abgrall [8], a simple second-order conservative TVD scheme combined with a second-order non-conservative scheme was presented in [9]. In which the stiffened gas EOS was considered in the

simulations of compressible multi-fluid flows. This study has been extended in [10] to include the general EOS to simulate real material interactions test problems, where the Euler equations were replaced by a multiphase flow model and each phase was governed by its own EOS. Shyue [11] used the compressible Euler equations and proposed an extension of the work presented in [9, 12] to include the van der Waals EOS by casting the stiffened and van der Waals EOSs in a modified form known as the general van der Waals EOS. The modified van der Waals EOS was used for modelling the mixing zone between the two fluids. This work was extended in [13] to include the general Mie-Grüneisen EOS. However, these extensions are complex, as the number of equations in the model increases depending on the number of parameters defining the EOS of the fluids being considered. Using the reduced five-equation model of Allaire et al. [14] which is similar to that derived by Kapila et al. [15], the results of [8, 9, 12] were extended in [16, 17] through the simulation of interfaces between compressible fluids with various equations of state including the Mie-Grüneisen EOS.

Although the five-equation model [14, 15, 18] satisfies the mechanical equilibrium by using single pressure and velocity, which enable the model to be written in a conservative form. The model possesses some significant computational difficulties, arise from the presence of the non-conservative equation of the evolution of the volume fraction. These difficulties are related to shock computations, maintaining positivity of the volume fraction and capturing accurately wave transmission across diffuse interfaces. These difficulties are due to the non-conservative model, the difficulties in the approximation of velocity divergence in the volume fraction evolution equation and the non-monotonic behaviour of sound speed, respectively [19]. To overcome these difficulties the six-equation model [15] was investigated in [19], by restoring the effects of pressure non-equilibrium in the volume fraction equation using two pressures and related pressure relaxation terms. Petitpas et al. [20] highlighted that when using complicated EOSs, they had to perform multiple adjustments to their algorithm. An attempt was made in [21] to construct a common framework for the general EOS, but their approach was different.

In this paper, the six-equation model [15] has been used here to consider various equations of state, including the more complex EOSs, i.e. van der Waals, Cochran-Chan, Jones-Wilkins-Lee (JWL) and shock wave EOSs, written in the general form of the Mie-Grüneisen EOS, without the need to do the modifications in the developed algorithm. The interfaces are captured rather than tracked using a developed diffuse interface method on a structured grid. The method is based on Godunov's approach to solve the hyperbolic part of the model using an extended HLL approximate Riemann solver described in [22] for single phase, which is modified and then extended to simulate compressible two-phase flow in two dimensions as given in [23]. To achieve a second-order accuracy, the MUSCL scheme is implemented with the Slope-Limiter.

2. The Compressible Two-Phase Flow Model

The compressible two-phase flow model, which is known as the six-equation model [19, 24], was derived by Kapila *et al.* [15] from the seven-equation model of Baer and Nunziato [25] in the asymptotic limit of zero velocity relaxation time. In this model, both fluids have the same velocity but each fluid has its own pressure. The model consists of the evolution equation for the volume fraction of one of the phases, the mass equations for each phase, a mixture momentum equation and the energy equations for each phase. The non-conservative hyperbolic model in two dimensions without heat and mass transfer and its closure relations are given in [23] and in one-dimensional form is written as follows:

$$\frac{\partial \alpha_1}{\partial t} + u\frac{\partial \alpha_1}{\partial x} = \mu(p - p\,), \tag{1a}$$

$$\frac{\partial \alpha_1 \rho_1}{\partial t} + \frac{\partial \alpha_1 \rho_1 u}{\partial x} = 0, \tag{1b}$$

$$\frac{\partial \alpha_2 \rho_2}{\partial t} + \frac{\partial \alpha_2 \rho_2 u}{\partial x} = 0, \tag{1c}$$

$$\frac{\partial \rho u}{\partial t} + \frac{\partial \left(\rho u_2 + \alpha_1 p_1 + \alpha_2 p_2\right)}{\partial x} = 0, \tag{1d}$$

$$\frac{\partial \alpha_1 \rho_1 e_1}{\partial t} + \frac{\partial \alpha_1 \rho_1 e_1 u}{\partial x} + \alpha_1 \rho_1 \frac{\partial u}{\partial x} = -\mu p_I \left(p_1 - p_2\right), \tag{1e}$$

$$\frac{\partial \alpha_2 \rho_2 e_2}{\partial t} + \frac{\partial \alpha_2 \rho_2 e_2 u}{\partial x} + \alpha_2 \rho_2 \frac{\partial u}{\partial x} = -\mu p_I \left(p_1 - p_2\right), \tag{1f}$$

where α_n, ρ_n, p_n and e_n are the volume fraction, the density, the pressure and the specific internal energy of phase n. The subscript n refers to the subscripts 1 and 2 that denote phases 1 and 2, respectively, p_I is the interfacial pressure, u is the x-component of the mixture velocity and ρ is the mixture density.

In the presence of shocks, inaccuracies in the thermodynamic state are expected because of the approximation of the two non-conservative internal energy equations. To correct these inaccuracies, an additional conservative total mixture energy equation was proposed in [19]. This equation is obtained by summing up the two internal energy equations with mass and momentum equations.

$$\frac{\partial \left(\rho e + \frac{1}{2}\rho u^2\right)}{\partial t} + \frac{\partial u \left(\rho e + \frac{1}{2}\rho u^2 + \alpha_1 p1 + \alpha_2 p2\right)}{\partial x} = 0, \tag{2}$$

where ρe the mixture internal energy is defined as $\rho e = \alpha_1 \rho_1 e_1 + \alpha_2 \rho_2 e_2$.

2.1 Equations of state (EOSs)

An equation of state for each phase is needed to relate the pressure with the density and the internal energy. The six-equation model is flexible and can deal with different equations of state for each phase. In order to deal with problems with different types of EOSs, we write various EOSs in the general form of the Mie-Grüneisen EOS as follows:

$$p(\rho, e) = \rho \, \Gamma_k(\rho)[e - e_k(\rho)] + p_k(\rho) \tag{3}$$

where $\Gamma_k(\rho)$, $e_k(\rho)$ and $p_k(\rho)$ are the material dependent functions, i.e. reference Grüneisen, internal energy and pressure. They are given for various EOSs in Table 1. With these reference functions, it is now feasible to simulate a diverse range of applications using different equations of state (EOSs) without the requirement for algorithm modifications.

1) Ideal gas EOS:

In the caloric ideal gas EOS, the pressure has the form

$$p = (\gamma - 1)\rho e, \tag{4}$$

where γ is the adiabatic specific heat ratio depending on the gas under consideration, $\gamma = c_p/c_v$. The parameters c_p and c_v are the specific heats at constant pressure and volume, respectively. By writing the ideal gas EOS (4) in the form of Mie-Grüneisen EOS (3), the reference material dependent functions are as given in Table 1. The adiabatic specific heat ratio for an ideal gas could also be calculated by the relation:

$$\gamma = \frac{m + 2}{m}$$

where m is the degrees of freedom of a molecule, for monatomic gases m = 3 and for diatomic gases m = 5.

2) Stiffened gas (SG) EOS:

The stiffened gas EOS can be used to obtain the behaviour of gases, liquids and compressible solids.

The pressure has the form

$$p = (\gamma - 1)\rho e - \gamma\pi, \tag{5}$$

where the parameters γ and π are constants that depend on the particular material under consideration. These parameters can be determined for various materials using the experimental data [26], following the procedure given in [27]. It can be notice that if the pressure constant $\pi = 0$, SG EOS reduces to the ideal gas EOS. By writing the SG EOS (5) in the form of the Mie-Grüneisen EOS (3), the reference material dependent functions are as given in Table 1.

3) van der Waal's gas EOS:

The van der Waal's gas EOS is used to govern real gases and can be written in the following form:

$$p = \left(\frac{\gamma - 1}{1 - b\rho}\right)(\rho e + a\rho^2) - a\rho^2, \tag{6}$$

where γ, a and b are constants that depend on the particular gas under consideration. van der Waal's EOS (6) may be rewritten in the form of the Mie-Grüneisen EOS (3), the reference material dependent functions are as given in Table 1.

4) Cochran-Chan EOS:

This EOS is widely used to describe solids under a high-pressure shock wave. It is more accurate than the SG EOS in such conditions [10]. The Cochran-Chan EOS may be written in the form of the Mie-Grüneisen EOS (3) as follows:

$$p = \rho(\gamma - 1)\left\{e + \frac{A_1}{\rho_o(1 - E_1)}\left[\left(\frac{\rho_o}{\rho}\right)^{1-E_1} - 1\right] - \frac{A_1}{\rho_o(1 - E_2)}\left[\left(\frac{\rho_o}{\rho}\right)^{1-E_2} - 1\right] + C_v T_o\right\} + $$
$$+ A_1\left(\frac{\rho_o}{\rho}\right)^{-E_1} - A_2\left(\frac{\rho_o}{\rho}\right)^{-E_2} \tag{7}$$

where γ, A_1, E_1, A_2, E_2, ρ_o, C_v and T_o are parameters that depend on the real material under consideration. The reference material dependent functions for the Cochran-Chan EOS are given in Table 1.

5) Jones-Wilkins-Lee (JWL) EOS:

This EOS is used to govern detonation products. The JWL EOS may be written in the form of the Mie-Grüneisen EOS (1) as follows:

$$p = \rho(\gamma - 1)\left\{e - \frac{A_1}{\rho_o R_1}e^{\left(-R_1\frac{\rho_o}{\rho}\right)} - \frac{A_2}{\rho_o R_2}e^{\left(-R_2\frac{\rho_o}{\rho}\right)} - C_{ek}\right\} + $$
$$A_1 e^{\left(-R_1\frac{\rho_o}{\rho}\right)} + A_2 e^{\left(-R_2\frac{\rho_o}{\rho}\right)} \tag{8}$$

where γ, A_1, R_1, A_2, R_2 and C_{ek} are constants that depend on the real material under consideration. The reference material dependent functions for the JWL EOS are given in Table 1.

6) Shock wave EOS:

This equation of state consists of the Mie-Grüneisen EOS (3) and:

$$U_s = c_0 + sU_p$$

where U_s is the shock velocity, c_0 is the speed of sound in the material under consideration at atmospheric conditions, U_p is the particle velocity and s is a dimensionless parameter. Experimental data for high pressure values are available for many materials in [28].

$$p = \rho(\gamma - 1)\left(\frac{\rho_o}{\rho}\right)^\alpha e - e_o - \left(\frac{C_o^2\left(1 - \frac{\rho_o}{\rho}\right)^2}{2\left[1 - s\left(1 - \frac{\rho_o}{\rho}\right)\right]^2}\right) +$$

$$p_o + \frac{\rho_o C_o^2\left(1 - \frac{\rho_o}{\rho}\right)}{\left[1 - s\left(1 - \frac{\rho_o}{\rho}\right)\right]^2} \tag{9}$$

The general form for the mixture EOS can be written as follows:

$$p(\rho_e, \alpha_1, \alpha_2) = \frac{\rho_e - \sum_n^2\left(\frac{\alpha_n(\rho_n\Gamma_k(\rho_n)e_k(\rho_n) - p_k(\rho_n))}{\Gamma_k(\rho_n)}\right)}{\sum_n^2\left(\frac{\alpha_n}{\Gamma_k(\rho_n)}\right)} \tag{10}$$

where ρe is the mixture internal energy and is defined as $\rho e = \sum_n^2 \alpha_n\rho_n e_n$ the other functions are given in Table 1 for each EOS.

3. Numerical Method

The numerical solution of the considered six-equation compressible multi-phase flow model is complicated owing to the presence of the non-conservative equation of volume fraction evolution, the non-conservative terms, and the relaxation and source terms in the model. Thus, the numerical solution of the model can be achieved by splitting the model into a hyperbolic part and a source and relaxation part. These different parts are solved in succession using the Strang splitting approach, which can symbolically be written as follows:

$$U_i^{n+1} = L_s^{\frac{\Delta t}{2}} L_h^{\Delta t} L_s^{\frac{\Delta t}{2}} U_i^n \tag{11}$$

The symbol $L_s^{\frac{\Delta t}{2}}$ represents the relaxation and source terms integration operators over half of the time interval. $L_h^{\Delta t}$ is the numerical solution operator of the hyperbolic part. U_i^n and U_i^{n+1} are the conservative vectors at the time levels n and n+1, respectively. The hyperbolic part is solved using an extended finite volume Godunov approach using the HLL approximate Riemann solver with the MUSCL scheme to achieve second-order accuracy as given in [22, 29]. The pressure relaxation is applied as given in [30].

4. Numerical Results

To assess the numerical performance of our approach, various compressible two-phase flow problems have been studied with either the same type of EOS or different types of EOS applied to each phase. All these types of EOSs are used in these problems to show the generality and the oscillation-free feature of the current method. In all test cases, a common assumption is made, that is a presence of a negligible volume fraction 10^{-8} of the other fluid in the fluid is considered a pure fluid. For all test cases, a mesh of 400 cells has been utilized.

Table 1. The Mie-Grüneisen EOS functions Table

EOS	$\Gamma_k(\rho)$	$e_k(\rho)$	$p_k(\rho)$
Ideal gas	$\gamma-1$	0	0
Stiffened gas	$\gamma-1$	$\dfrac{\pi}{\rho}$	$-\pi$
van der Waals	$\dfrac{\gamma-1}{1-b\rho}$	$-a\rho$	$-a\rho^2$
Cochran-Chan	$\gamma-1$	$-\dfrac{A_1}{\rho_o(1-E_1)}\left[\left(\dfrac{\rho_o}{\rho}\right)^{1-E_1}-1\right]+\dfrac{A_1}{\rho_o(1-E_2)}\left[\left(\dfrac{\rho_o}{\rho}\right)^{1-E_2}-1\right]-C_vT_o$	$A_1\left(\dfrac{\rho_o}{\rho}\right)^{-E_1}-A_2\left(\dfrac{\rho_o}{\rho}\right)^{-E_2}$
JWL	$\gamma-1$	$\dfrac{A_1}{\rho_oR_1}e^{(-R_1\frac{\rho_o}{\rho})}-\dfrac{A_2}{\rho_oR_2}e^{(-R_2\frac{\rho_o}{\rho})}-C_{ek}$	$A_1e^{(-R_1\frac{\rho_o}{\rho})}+A_2e^{(-R_2\frac{\rho_o}{\rho})}$
Shock wave	$(\gamma-1)\left(\dfrac{\rho_o}{\rho}\right)^{\alpha}$	$e_o+\dfrac{C_o^2\left(1-\frac{\rho_o}{\rho}\right)^2}{2\left[1-s\left(1-\frac{\rho_o}{\rho}\right)\right]^2}$	$p_o+\dfrac{\rho_oC_o^2\left(1-\frac{\rho_o}{\rho}\right)}{\left[1-s\left(1-\frac{\rho_o}{\rho}\right)\right]^2}$

4.1 One-dimensional test problems

1) Advection test problem

The first test is a popular interface advection test [20]. The computational domain consists of a 1 m tube in length containing water on the left and air on the right. Initially, the interface is located at a distance of 0.5 m. The initial data and the stiffened gas EOS parameters for both fluids are:

$$(\rho, u, p, \gamma) = \begin{cases} 1000, 100, \ 10^5, 4.4, 6 \times 10^8 & \text{if } x \leq 0.5 \\ 50, 100, \ 10^5, 1.4, 0 & \text{if } x > 0.5 \end{cases}$$

The results illustrated in Figure 1 are obtained at time t = 2.79 ms after 2203 time steps using a Courant-Friedrichs-Lewy (CFL) number equal to 0.9. The test shows the perfect behaviour of the method regarding preserving constant velocity and pressure profiles. A good agreement is achieved between the numerical solution (circles) and the exact solution (line).
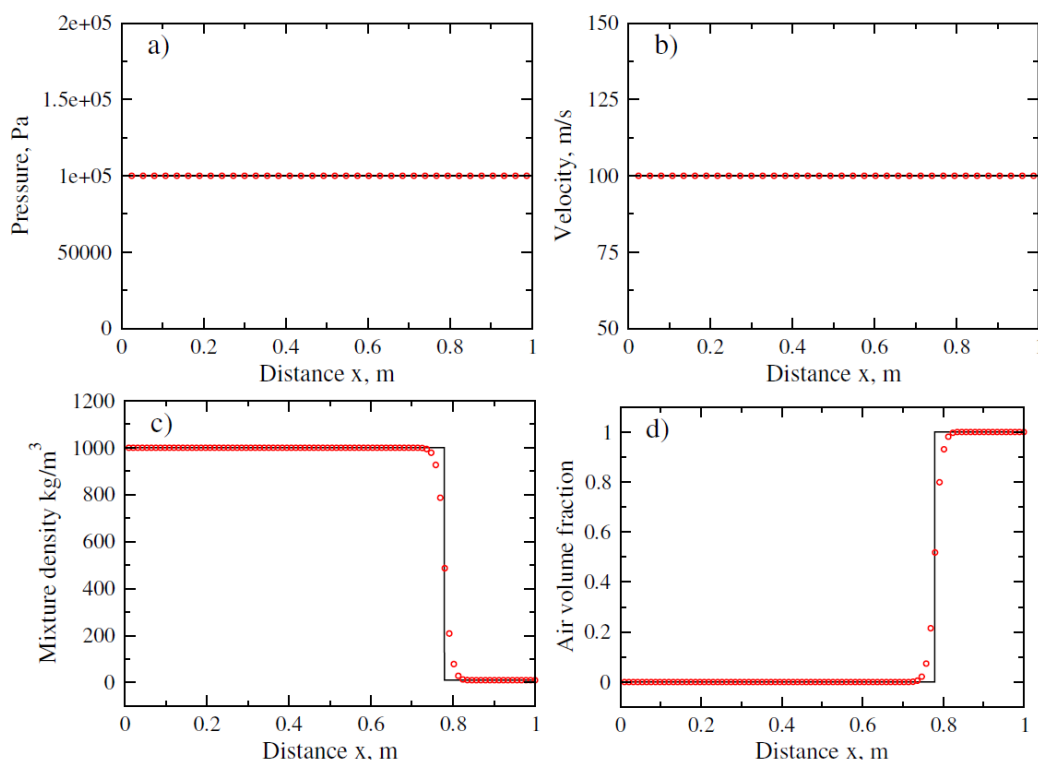

Figure 1. Advection test: (a) Pressure. (b) Velocity. (c) Mixture density. (d) Air volume fraction. Numerical solution (circles) and exact solution (line) at t = 2.79 ms.

2) Air-gas shock tube test problem

The second test is conducted on the same domain as the first test. In the air-gas shock tube test problem, the initial discontinuity that separates the two gases is located at *x* = 0.5 m. The air on the left-hand side of the tube has a higher pressure. Both gases are initially at rest. Air is governed by the van der Waals EOS (6), and its constant parameters are γ = 1.4, a = 5, b = 10^{-3}, whereas the other gas is governed by the SG EOS (5), and its constant parameters are γ = 1.2,   π = 0. The initial conditions are as follows:

$$(\rho, u, p) = \begin{cases} 1, 0, \ 10^5 & \text{if } x \leq 0.5 \\ 0.125, 0, \ 10^4 & \text{if } x > 0.5 \end{cases}$$

A shock wave propagates to the right from the higher density gas to the lower density gas, and a rarefaction wave propagates to the left. The results shown in Figure 2 are obtained at   *t* = 0.0007 s after 351 time steps using a CFL number equal to 0.9. Also, a good agreement is achieved between the numerical solution (circles) and the exact solution (line) taken from [31].
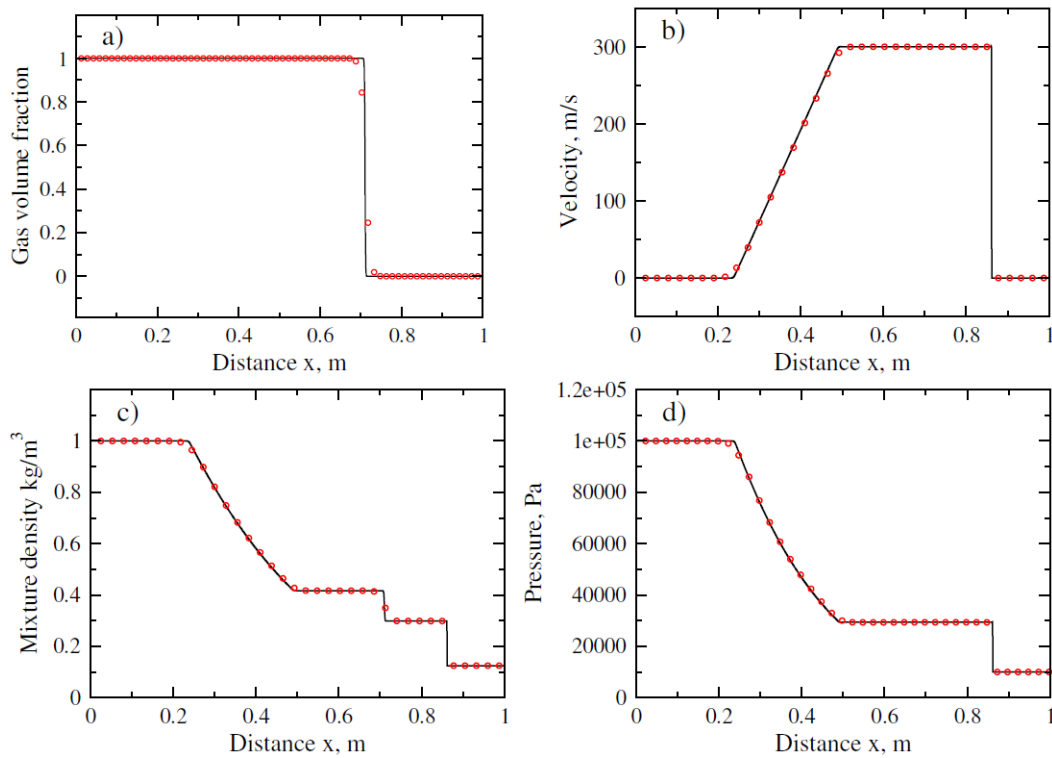
Figure 2. Air-gas shock tube test: (a) Air volume fraction. (b) Velocity. (c) Mixture density. (d) Pressure. Numerical solution (circles) and exact solution (line) at t = 0.0007 s.

3) Water-air shock tube test problem

The third test is a standard water-air shock tube of 1 m length filled with water under high pressure on the left and air on the right at atmospheric pressure, and both fluids are at rest. The initial discontinuity that separates liquid and gas is located at $x = 0.7$ m. The water is governed by the SG EOS (5), and its constant parameters are $\gamma = 4.4$, $\pi = 6 \times 10^8$, whereas air is governed by the van der Waals EOS (6), and its constant parameters are $\gamma = 1.4$, a = 5, b = 10^{-3}. The initial conditions are as follows:

$$(\rho, u, p) = \begin{cases} 1000, 0, \ 10^9 & \text{if } x \leq 0.7 \\ 50, 0, \ 10^5 & \text{if } x > 0.7 \end{cases}$$

In this test, a strong shock wave with a pressure ratio of 10,000 propagates to the right from the high-density fluid to the low-density fluid, and a rarefaction wave propagates to the left. Figure 3 shows the results of air volume fraction (a), velocity (b), mixture density (c), and pressure (d). The results are obtained at time t = 229 μs after 275 time steps using a CFL number equal to 0.9 with 400 cells.

Also, a good agreement is achieved between the numerical solution (circles) and the exact solution (line) taken from [9].
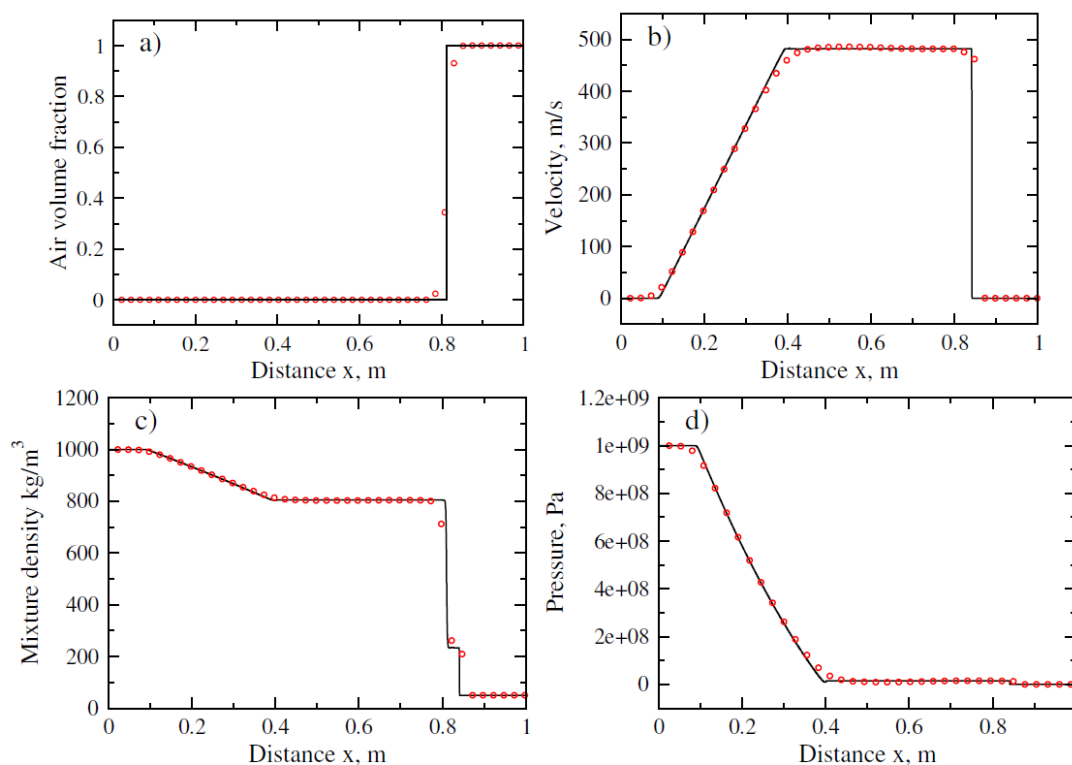
Figure 3. Water-air shock tube test: (a) Air volume fraction. (b) Velocity. (c) Mixture density. (d) Pressure. Numerical solution (circles) and exact solution (line) at t = 229 μs.

4) Solid impact test problem

The fourth test simulates the impact of a copper plate with a solid inert explosive. Both materials are governed by the Cochran-Chan EOS (7) and are modelled in a computational domain of 1 m in length. The copper is put on the left-hand side, and the explosive material is put on the right-hand side of the computational domain. The material interface initially located at $x = 0.5$ m. While the copper plate has an initial velocity of 1500 m/s to the right, the explosive material is at rest. Both materials are at atmospheric pressure, with the initial densities and EOS parameters given in Table 2.

Table 2. Materials Properties for the Cochran-Chan EOS.

Parameter	Copper	Explosive
ρ_0, $[kg/m^3]$	8900	1840
C_v, $[J/kg \cdot K]$	393	1087
A_1, $[Pa]$	1.45667×10^{11}	1.2871×10^{10}
A_2, $[Pa]$	1.47751×10^{11}	1.34253×10^{10}
E_1	2.994	4.1
E_2	1.994	3.1
T_0	300	300
γ	3	1.93

The solution to this test problem consists of two shock waves. The first is propagating to the right in the inert explosive, and the second is propagating to the left in the copper. Figure 4 shows the results of pressure (a), velocity (b), mixture density (c), and temperature (d). The results are obtained at time $t = 85$ μs after 461 time steps using a CFL number equal to 0.5. In detonation problems, it is important

to report the solution of the detonation temperature, which is calculated for each phase individually as follows:

$$T_n = \frac{e_n}{C_{vn}} \qquad\qquad n = 1, 2. \qquad\qquad (12)$$

The interfacial temperature can be calculated using the following relation:

$$T = \frac{\sum_n^2 \alpha_n \rho_n \, C_{vn} T_n}{\sum_n^2 \alpha_n \rho_n \, C_{vn}} \qquad\qquad (13)$$

Again, a good agreement is obtained between the numerical solution (circles) and the exact solution (line) taken from [9].
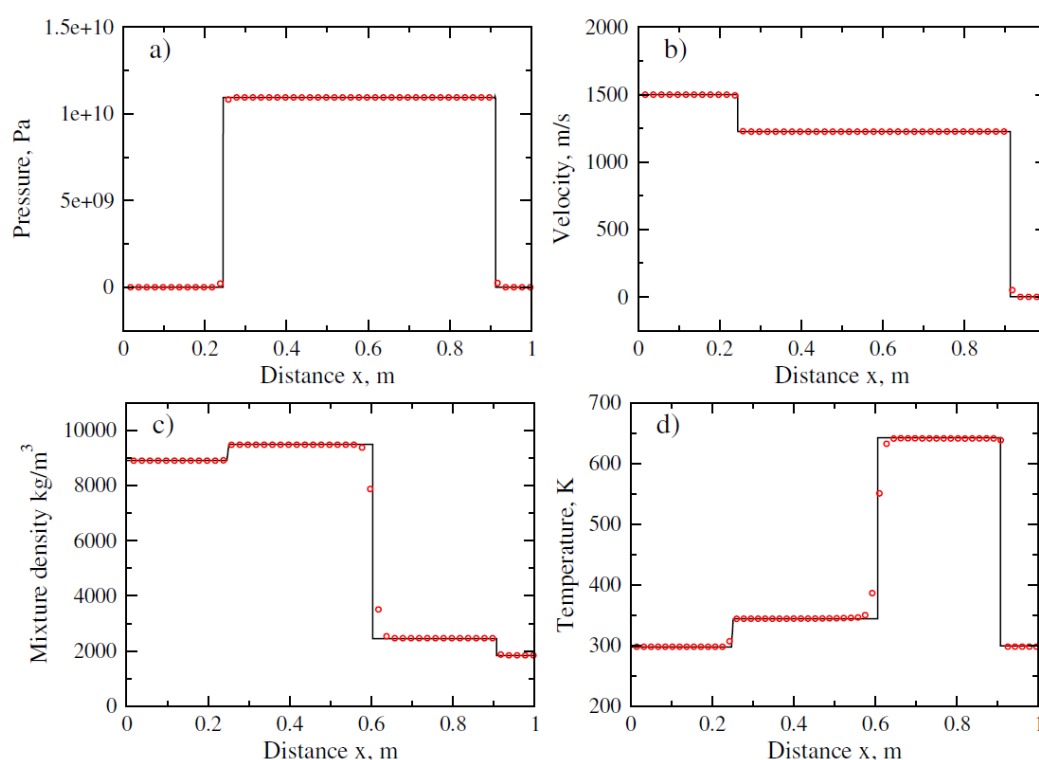

Figure 4. Solid impact test: (a) Pressure. (b) Velocity. (c) Mixture density. (d) Temperature. Numerical solution (circles) and exact solution (line) at t = 85 μs.

5) Detonation products-copper interaction test problem

The final one-dimensional test problem is an interaction of detonation products with solid copper. The detonation products are governed by a more complex EOS, i.e., the Jones-Wilkins-Lee EOS (8), and the copper is governed by the Cochran-Chan EOS (7). Both materials are modelled in a computational domain of 1 m in length. While the detonation products of TNT explosive are put on the left-hand side, the copper is put on the right-hand side. The material interface is initially located at x = 0.5 m. The initial conditions, taken from [9, 13], are as follows:

$$(\rho, u, p) = \begin{cases} 2485.37, 0, \, 3.7 \times 10^{10} & \text{if } x \leq 0.5 \\ 8900, 0, \, 10^5 & \text{if } x > 0.5 \end{cases}$$

The EOS parameters for copper are the same as for the previous test problem in Table 2, but those for the detonation products governed by JWL EOS are ρ_o = 1840 kg/m^3, A_1 = 8.545 × 10^{11} Pa, R_1 = 4.6, A_2 = 2.05 × 10^{10} Pa, R_2 = 1.35, C_v = 815 J/(kg K), γ = 1.25, and C_{ek} = 0.

The solution to this test problem consists of a shock wave propagating to the right in the copper, and a rarefaction wave propagating to the left in the inert explosive. Figure 5 shows the results of pressure

(a), velocity (b), mixture density (c), and temperature (d). The results are obtained at time $t = 73$ µs after 348 time steps using a CFL number equal to 0.6.
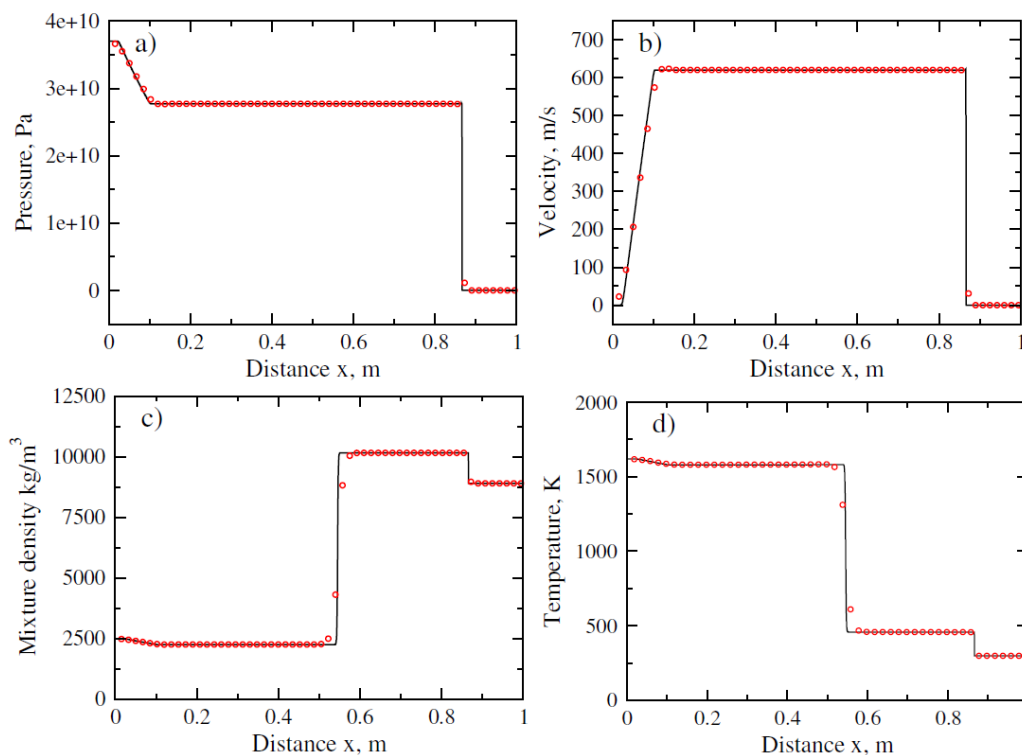

Figure 5. Detonation product-copper interaction test: (a) Pressure. (b) Velocity. (c) Mixture density. (d) Temperature. Numerical solution using 400 cells (circles) and 10,000 cells (line) at t = 73 µs.

4.2 Two-dimensional test problems

1) Gas bubble underwater explosion

The gas bubble underwater explosion test is an explosion of a gas bubble at high pressure under water. A circular gas bubble of radius $r_o = 0.2$ m is located at the centre of a square computational domain of 1 m × 1 m. While the top and bottom boundaries of the domain are set to be periodic boundary conditions, the left and right boundaries of the domain are set to be extrapolation boundary conditions. The water is governed by the SG EOS (5) and its constant parameters are $\gamma = 4.4$, $\pi = 6 \times 10^8$, whereas the gas is governed by the van der Waals EOS (6) and its constant parameters are $\gamma = 1.4$, a = 1, b = 10^{-4}. The initial conditions are as follows:

$$(\rho, u, p) = \begin{cases} 1250, 0, 10^9 & \text{if } r \leq 0.2 \\ 1000, 0, 10^5 & \text{if } r > 0.2 \end{cases}$$

When the explosion of the gas bubble starts, an outward strong shock wave is transmitted to the surrounding water, an inward rarefaction wave propagates in the gas, and a contact discontinuity continues to separate the gas and water. Figure 6 shows a surface plot for the mixture density and pressure at time $t = 120$ µs after 436 time steps using a CFL number equal to 0.3 with 300 × 300 cells. Figure 7 shows the cross-section plot of the pressure and mixture density for the gas bubble under-water explosion test at y = 0.5 m and t = 120 µs.
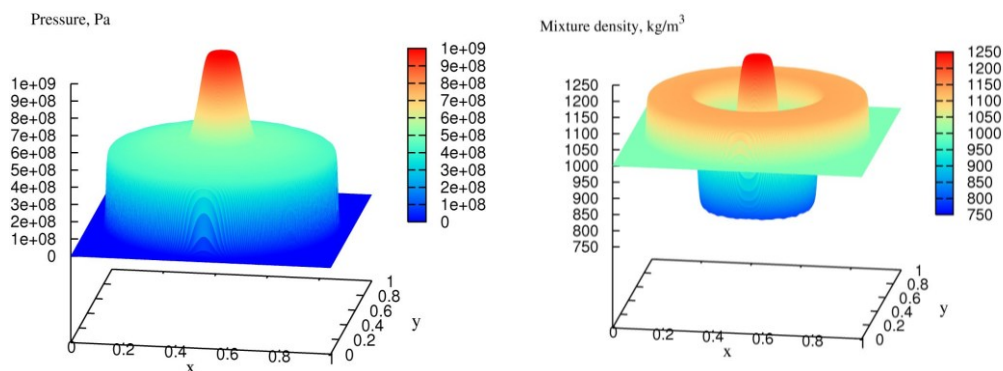
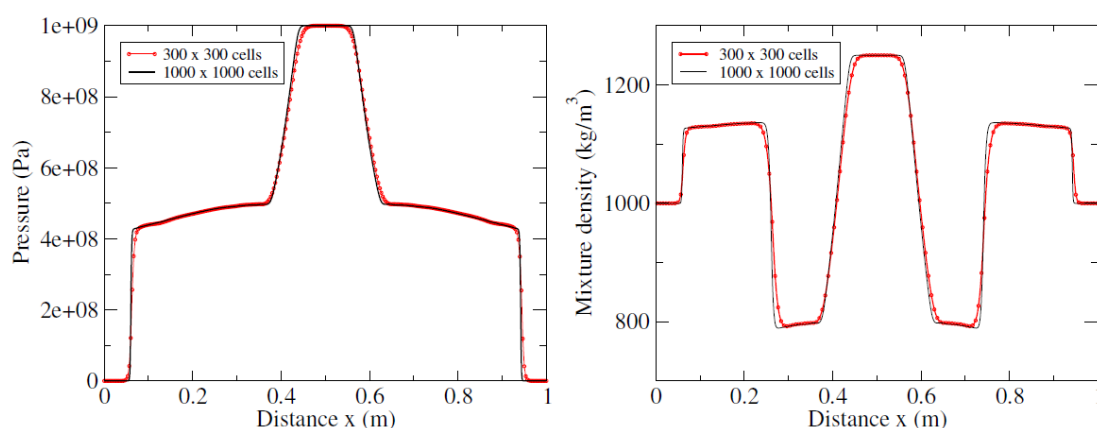Figure 6. Pressure and mixture density for gas bubble underwater explosion test at t = 120 μs.

Figure 7. Cross-section plot of the pressure and mixture density for gas bubble under- water explosion test at y = 0.5 m and t = 120 μs (Cercles) current results, (Line) exact solution.

2) R22 bubble-air shock interaction

The R22 bubble-air shock interaction was examined experimentally in [32], and numerically for example, in [32, 33], in order to assess the performance of numerical methods. The initial configuration of the computational domain is shown in Figure 8. While reflective boundary conditions are employed on the upper and lower boundaries, extrapolation boundary conditions are employed on the left and right boundaries. The incident shock wave is located on the right side of the R22 cylindrical bubble and travels in air at M=1.22 to the left. The bubble is assumed to be in thermodynamic and mechanical equilibrium with the surrounding air. We consider the bubble and the surrounding air (pre-shock air) to be at atmospheric pressure and temperature (101325 Pa and 25). The air and R22 properties used for this simulation are given in Table 3.

In what follows the subscripts 1, 2 and 3 denote pre-shocked zone, bubble and post-shocked zone, respectively. The bubble density ρ_2 can be calculated as follows:

$$\rho_2 = \rho_1 \frac{R_1}{R_2} \tag{14}$$

The density, pressure and velocity of the post-shocked zone can be calculated according to [22] as:

$$\rho_3 = \rho_1 \frac{(\gamma_1 + 1)(M_1 - M_3)^2}{(\gamma_1 - 1)(M_1 - M_3)^2 + 2} \tag{15}$$

$$p_3 = p_1 \frac{2\gamma_1(M_1 - M_3)^2 - (\gamma_1 - 1)}{(\gamma_1 + 1)} \tag{16}$$
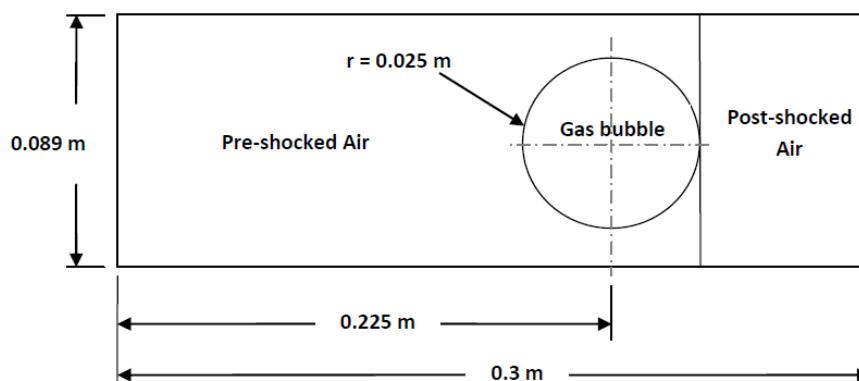
Figure 8. Initial configuration for air shock interactions with R22 and Helium bubbles.

Table 3. Gases properties used for the shock-bubble interactions.

Gas	γ	R [J/kg·K]	C_v [J/kg]
K Air	1.4	0.287	0.72
R22	1.249	0.091	0.365
He + 28 % air	1.648	1.578	2.44

The speed of sound in air is given by

$$c = \sqrt{\frac{\gamma_1 p_1}{\rho_1}} \tag{17}$$

Knowing the Mach number, the shock wave speed S can be calculated from:

$$S = M_3 c \tag{18}$$

The velocity of air in the post-shocked zone is

$$u_3 = \left(1 - \frac{\rho_1}{\rho_3}\right) S + u_1 \frac{\rho_1}{\rho_3} \tag{19}$$

The initial conditions and the constant parameters for the SG EOS governing air and R22 bubble are given in Table 4.

The numerical results of the mixture density using an idealised Schlieren function for the R22 bubble and the surrounding air are shown in Figure 9 using a mesh size of 1500 × 445 cells and a CFL number equal to 0.3 at times 55, 115, 135, 187, 247, 318, 342, 417, and 1020 μs. In this test, both gases are governed by the SG EOS.

Table 4. Initial conditions and the SG EOS parameters for the R22 bubble test.

Physical property	Air	R22	Air
Density, kg/m³	1.1839	3.734	1.6295
velocity u, m/s	0	0	-115.478
velocity v, m/s	0	0	0
Pressure, Pa	101325	101325	159060
γ	1.4	1.648	1.4
π	0	0	0

Similar results to Figure 9 were obtained when air is governed by the van der Waals EOS. This means that the van der Waals EOS reduces to the ideal gas EOS.
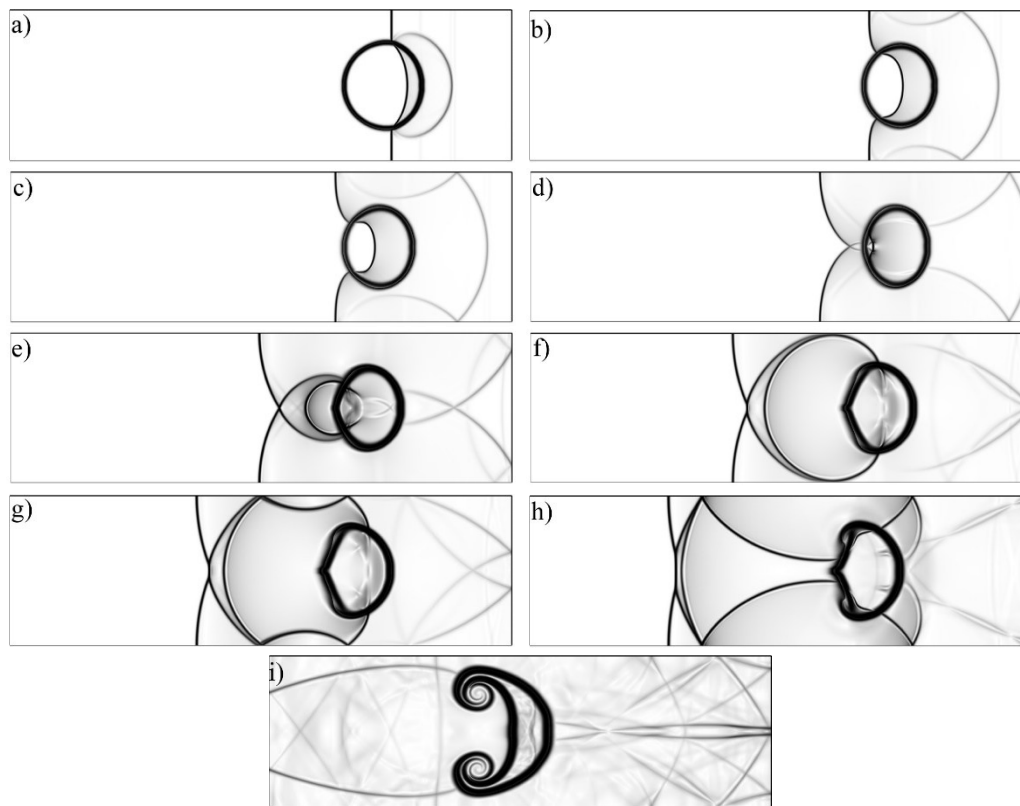

Figure 9. The mixture density using idealised Schlieren function for R22 bubble-air shock interaction at times: (a) 55 μs, (b)115 μs, (c) 135 μs, (d) 187 μs, (e) 247 μs, (f) 318 μs, (g) 342 μs, (h) 417 μs and (i) 1020 μs.

The *x-t* diagram shown in Figure 10 gives the position history of the upstream and downstream edges of the R22 bubble as well as the refracted, incident, and transmitted shock waves. The schematic diagram on the right part of Figure 10 shows the points used to construct the *x-t* diagram. All positions are measured at the axis of symmetry except for the incident shock wave, which is measured either at the top or bottom boundaries of the domain. Since our numerical method is diffusive, the points were measured at the mean thickness of the interface. The computed mean velocities compared to the experimental results of Haas and Sturtevant [32] and Quirk and Karni [33] are given in Table 5. These results are in very good agreement with the experimental results of [32] and other numerical results of [33]. A maximum estimated error of -1.9% is computed compared to the experimental results.

Table 5: A comparison of the computed velocities for the R22 bubble case with experimental results of [32] and numerical results of [33]; for key, see Figure 10

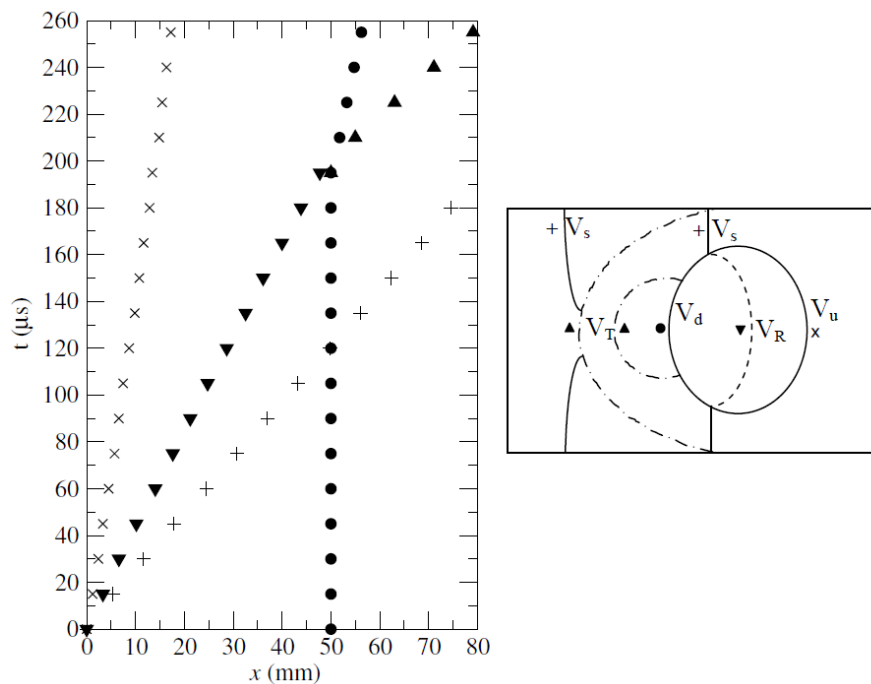| Velocity	V_s	V_R	V_T	V_u	V_d
Experiment [32]	415	240	540	73	78
Qurik and Karni [33]	420	254	560	70	82
% Error	+1.2	+5.8	+3.7	-4.1	+5.1
Current	414.32	235.37	536.13	71.6	78.45
% Error	-0.16	-1.9	-0.7	-1.9	+0.57

Figure 10. $x - t$ diagram for R22 bubbles (left), key points (right): V_s incident shock;
V_R refracted shock; V_T transmitted shock; V_u upstream edge; V_d downstream edge.

3) Helium bubble-air shock interaction

The helium bubble-air shock interaction was examined experimentallyin [32, 35], and numerically for example, in [31, 33, 36, 37, 38]. In thistest, a helium bubble was hit by a planar shock moving in air with a 1.22 Mach number. The initial configuration of the computational domain and the boundary conditions are as in the previous test; see Figure 8. The helium bubble is contaminated with 28% air. Gases properties used for the simulations are given in Table 3. The initial conditions were calculatedin the same manner as given in the previous test. The initial conditions andthe constant parameters for the van der Waals and SG EOSs governing air and the helium bubble, respectively, are given in Table 6.

Table 6: Helium test initial conditions and the van der Waals and SG EOSs parameters

Physical property	Air pre-shock	He+28% air bubble	Air post-shock
Density, [kg/m³]	1.1839	0.2153	1.6295
velocity u, [m/s]	0	0	-115.478
velocity v, [m/s]	0	0	0
Pressure, [Pa]	101325	101325	159060
γ	1.4	1.648	1.4
π [Pa]	0	0	0
a, [Pa · m⁶/kg]	5	0	5
b, [m⁶/kg]	10^{-3}	0	10^{-3}

The numerical results of the mixture density using the idealized Schlieren function for the helium

bubble and the surrounding air are shown in Figure 11 using a mesh size of 1500 × 445 cells and a CFL number equal to 0.3 at times 28, 44, 58, 72, 82, 102, 245, 427, 674, and 983 μs. In this test, the helium bubble is governed by the SG EOS, and the air is considered as a real gas, i.e., governed by the van der Waals EOS. These results are in very good agreement with the experimental results [30] and the other numerical results [31, 29, 34, 35, 36]. The same results were obtained when both gases were governed by the SG EOS. This confirms that the van der Waals EOS reduces to the ideal gas EOS in this condition.

The position history of the interaction between the incident shock and the helium bubble is shown in Figure 12. The figure indicates the *x* positions of the upstream and downstream edges of the helium bubble as well as therefracted, incident, and transmitted shock waves. The schematic diagram on the right part of Figure 12 shows the points used to construct the *x-t* diagram. All positions are measured at the axis of symmetry except for the incident shock wave and the upstream edge, i.e., the incident shock wave is measured either at the top or bottom boundaries of the domain, and the upstream edge is measured at 0.0214 above the axis of symmetry. Since our numerical method is diffusive, the points were measured at the mean thickness of the interface. The computed mean velocities compared to the experimental results [31] and numerical results [32, 35] are given in Table 7. These results are in very good agreement with the experimental results, with a maximum estimated error of -1.9%.

Table 7: A comparison of the computed velocities for the He+28% air bubble case with experimental results [31], and numerical results [32, 35]; for key, see Figure 12

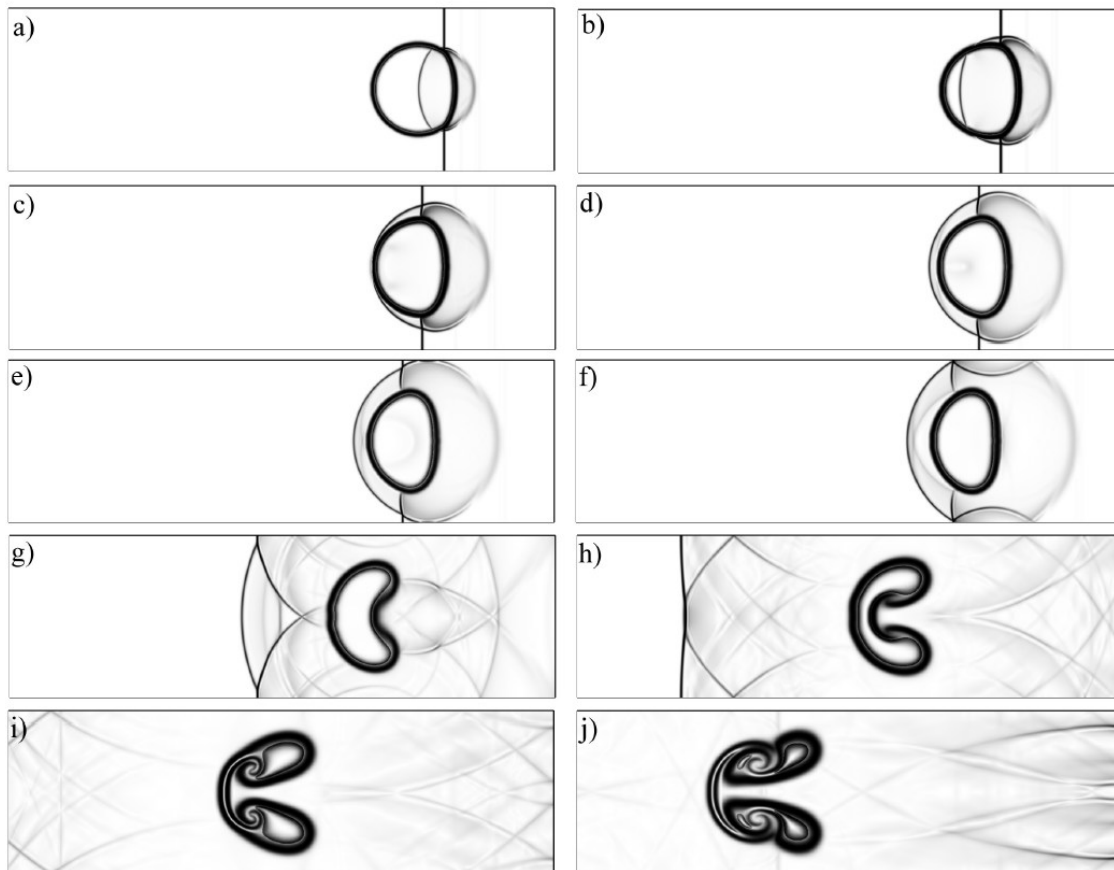| **Velocity**	$\mathbf{V_s}$	$\mathbf{V_R}$	$\mathbf{V_T}$	$\mathbf{V_u}$	$\mathbf{V_d}$	$\mathbf{V_j}$
Experiment [31]	410	900	393	170	145	230
Qurik and Karni [32]	422	943	377	178	146	227
% Error	+2.9	+4.8	+4.1	+4.7	+0.7	-1.3
Marquina and Mulet [35]	414	943	373	176	153	229
% Error	+1	+4.8	-5.4	+3.4	+5.2	-0.4
Current	407.4	904.64	377.68	166.23	144	223.58
% Error	+0.63	+0.52	-3.9	-2.2	-0.69	-2.8

Figure 11: The mixture density using idealised Schlieren function for Helium + %28 air bubble-air shock interaction at times: (a) 28 μs, (b) 44 μs, (c) 58 μs, (d) 72 μs, (e) 82 μs, (f) 102 μs, (g) 245 μs, (h) 427 μs (i) 674μs and (j) 983 μs.
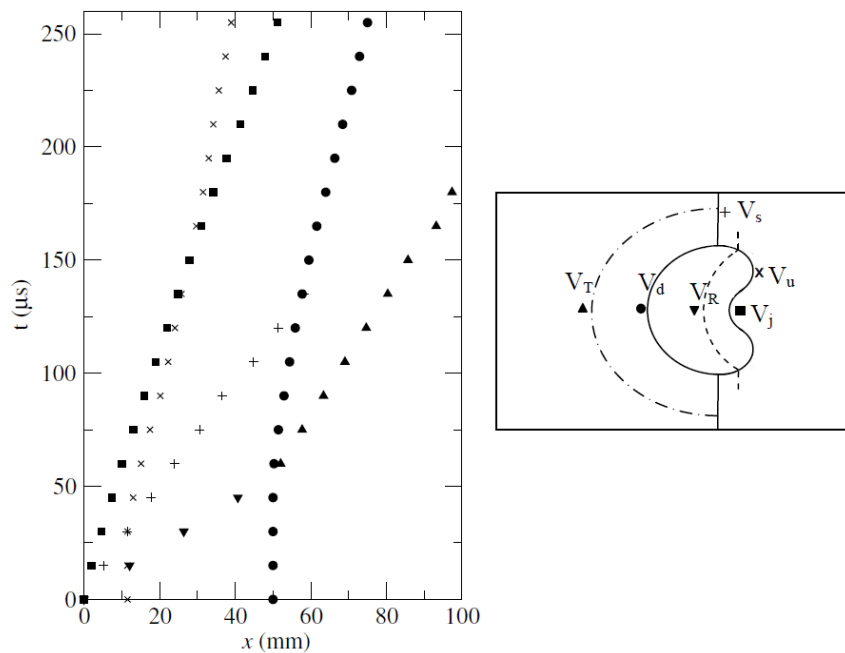

Figure 12: *x−t* diagram for He + 28% air bubbles (left), key points (right): V_s incident shock; V_R refracted shock; V_T transmitted shock; V_u upstream edge; V_d downstream edge and V_j air jet head.

5. Conclusions

This study has considered numerical simulations of multiphase flow using the six-equation model with various equations of state. All types of equations of state studied in this work were written in the general form of the Mie-Grüneisen EOS. A diffuse interface method on a structured mesh was used to solve the multiphase flow model. The developed numerical method has been based on a multiphase Godunov approach with HLL Riemann solver. The accuracy of the method is examined through carefully selected test problems in one and two-dimensional space. The method handles the simulation of the investigated two-phase flows very well with either the same type of EOS or different types of EOS. One-dimensional test problems were compared with the exact solution and the two-dimensional bubble shock interaction test.

REFERENCES

[1]   R. Saurel, J. Massoni, On Riemann-problem-based methods for detonations in solid energetic materials, International Journal for Numerical Methods in Fluids 26 (1) (1998) 101–121.

[2]   R. Nourgaliev, T. Dinh, T. Theofanous, Adaptive characteristics-based matching for compressible multifluid dynamics, Journal of Computational Physics 213 (2) (2006) 500 – 529.

[3]   S. Y. Kadioglu, M. Sussman, Adaptive solution techniques for simulating underwater explosions and implosions, Journal of ComputationalPhysics 227 (3) (2008) 2083 – 2104.

[4]   Ziyang Huang and Eric Johnsen, A consistent and conservative Phase-Field method for compressible multiphase flows with shocks, Journal of Computational Physics, (488), (2023). 112195.

[5]   B. Larrouturou, How to preserve the mass fractions positivity when computing compressible multi-component flows, Journal of Computational Physics 95 (1) (1991) 59 – 84.

[6]   S. Karni, Multicomponent flow calculations by a consistent primitive algorithm, Journal of Computational Physics 112 (1) (1994) 31 – 43.

[7]   S. Karni, Hybrid multifluid algorithms, Journal of Scientific Computing 17 (5) (1996) 1019–1039.

[8]   R. Abgrall, How to prevent pressure oscillations in multicomponent flow calculations: A quasi conservative approach, Journal of Computational Physics 125 (1) (1996) 150 – 160.

[9]   R. Saurel, R. Abgrall, A simple method for compressible multifluid flows,SIAM J. Sci. Comput. 21 (3) (1999) 1115–1145.

[10] R. Saurel, R. Abgrall, A multiphase Godunov method for compressible multifluid and multiphase flows, Journal of Computational Physics 150 (2) (1999) 425– 467.

[11] K.-M. Shyue, A fluid-mixture type algorithm for compressible multi- component flow with van der waals equation of state, J. Comput. Phys.156 (1) (1999) 43–88.

[12] K. Shyue, An efficient shock-capturing algorithm for compressible multi- component problems, Journal of Computational Physics 142 (1) (1998) 208–242.

[13] K.-M. Shyue, A fluid-mixture type algorithm for compressible multi- component flow with Mie–Grüneisen equation of state, Journal of Computational Physics 171 (2) (2001) 678 – 707.

[14] G. Allaire, S. Clerc, S. Kokh, A five-equation model for the numerical simulation of interfaces in two-phase flows, C. R. Acad. des Sci. Paris - Séries I: Mathematics 331 (12) (2000) 1017–1022.

[15] A. K. Kapila, R. Menikoff, D. Stewart, Two-phase modeling of deflagration-to-detonation transition in granular materials: Reduced equations, Physics of Fluids 13 (10) (2001) 3002–3024.

[16] G. Allaire, S. Clerc, S. Kokh, A five-equation model for the simulation of interfaces between compressible fluids, Journal of Computational Physics 181 (2) (2002) 577–616.

[17] H. W. Zheng, C. Shu, Y. T. Chew, N. Qin, Oscillation-free adaptive simulation of compressible two-fluid flows with different types of equation of state, in: F. Nicolleau, C. Cambon, J.-M. Redondo, J. Vassilicos, M. Reeks, A. Nowakowski (Eds.), New Approaches in Modeling Multiphase Flows and Dispersion in Turbulence, Fractal Methods and Syn- thetic Turbulence, Vol. 18 of ERCOFTAC Series, Springer Netherlands,(2012), 103–117.

[18] Mohamad Aslani, Jonathan D. Regele, A localized artificial diffusivity method to simulate compressible multiphase flows using the stiffened gas equation of state, Numerical methods in fluids, (88), (9) (2018), 413-433.

[19] R. Saurel, F. Petitpas, R. Berry, Simple and efficient relaxation methods for interfaces separating compressible fluids, cavitating flows and shocks in multiphase mixtures, Journal of Computational Physics 228 (5) (2009) 1678–1712.

[20] F. Petitpas, E. Franquet, R. Saurel, O. Le Métayer, A relaxation- projection method for compressible flows. part II: Artificial heat ex- changes for multiphase shocks, J. Comput. Phys. 225 (2) (2007) 2214– 2248.

[21] Zheng, H. W., C. Shu, Y. T. Chew and N. Qin. 2011. A solution adaptive simulation of compressible multi-fluid flows with general equation of state." Int. J. for Numer. Methods in Fluids 67(5):616-637.

[22] E. Toro, RIEMANN SOLVERS AND NUMERICAL METHODS FOR FLUID DYNAMICS:A PRACTICAL INTRODUCTION, Springer, 2009.

[23] Jolgam, S. A., Ballil, A. R., Nowakowski, A. F., & Shati, A. K. A, A quantitative numerical study for the interaction of strong shock waves with heterogeneous bubbles, 7 (1) (2020) 42 – 49.

[24] A. Zein, M. Hantke, G. Warnecke, Modeling phase transition for compressible two-phase flows applied to metastable liquids, Journal of Computational Physics 229 (2010) 2964–2998.

[25] M. R. Bear, J. Nunziato, A two-phase mixture theory for the deflagration to detonation transition DDT in reactive granular materials, Int. J. Multiphase Flow 12 (1986) 861–889.

[26] S. P. Marsh, LASL shock Hugoniot data, Univ. of California Press, Berkeley, 1980.

[27] J. Cocchi, R. Saurel, J. Loraud, Treatment of interface problems with Godunov-type schemes, Shock Waves 5 (1996) 347–357.

[28] Marsh, S. P. LASL SHOCK HUGONIOT DATA. Univ. of California Press, Berkeley (1980)

[29] A. Harten, P. Lax, B. van Leer, On upstream differencing and Godunov- type schemes for hyperbolic conservation laws, SIAM Review 25 (1) (1983) 35–61.

[30] M. H. Lallemand, A. Chinnayya, O. Le Métayer, Pressure relaxation procedures for multiphase compressible flows, International Journal forNumerical Methods in Fluids 49 (1) (2005) 1–56.

[31] R. Fedkiw, T. Aslam, B. Merriman, S. Osher, A non-oscillatory Eulerianapproach to interfaces in multi-material flows (the Ghost Fluid Method),Journal of Computational Physics 152 (2) (1999) 457– 492.

[32] J. F. Haas, B. Sturtevant, Interaction of weak shock waves with cylindrical and spherical gas inhomogeneities, Journal of Fluid Mechanics 181 (1987) 41–76.

[33] J. J. Quirk, S. Karni, On the dynamics of a shock-bubble interaction, Journal of Fluid Mechanics 318 (1996) 129–163.

[34] S. Qamar, G. Warnecke, Simulation of multicomponent flows using high order central schemes, Applied Numerical Mathematics 50 (2) (2004) 183 – 201.

[35] G. Layes, O. Le Métayer, Quantitative numerical and experimental studies of the shock accelerated heterogeneous bubbles motion, Physics of Fluids 19 (2007) 042105.

[36] A. Marquina, P. Mulet, A flux-split algorithm applied to conservative models for multicomponent compressible flows, Journal of Computational Physics 185 (1) (2003) 120 – 138.

[37] J. Giordano, Y. Burtschell, Richtmyer-Meshkov instability induced by shock-bubble interaction: Numerical and analytical studies with experimental validation, Physics of Fluids 18 (2006) 036102.

[38] H. Terashima, G. Tryggvason, A front-tracking/ghost-fluid method for fluid interfaces in compressible flows, Journal of Computational Physics228 (11) (2009) 4012 – 4037.